ELSEVIER

Journal of Molecular Catalysis A: Chemical 162 (2000) 67–82

JOURNAL OF MOLECULAR CATALYSIS A: CHEMICAL

www.elsevier.com/locate/molcata

Partially decarbonylated tetrairidium clusters on MgO: structural characterization and catalysis of toluene hydrogenation

Oleg S. Alexeev *, Do-Woan Kim, Bruce C. Gates [1]

Department of Chemical Engineering and Materials Science, University of California, Davis, CA 95616, USA

Abstract

Supported $[HIr_4(CO)_{11}]^-$, prepared by adsorption of $[Ir_4(CO)_{12}]$ from *n*-pentane solution onto MgO powder that had been partially dehydroxylated in vacuum at 400°C, was identified by infrared and extended X-ray absorption fine structure (EXAFS) spectroscopies. The clusters were decarbonylated to various degrees by treatment in He or H_2 and characterized by infrared and EXAFS spectroscopies. When the decarbonylation was carried out in H_2, the iridium aggregated; infrared data show that the CO ligands reacted with H_2, resulting in the formation of water and hydrocarbons. When the decarbonylation was carried out in He, the tetrahedral cluster frame remained unchanged; the fully decarbonylated clusters, modeled as Ir_4 tetrahedra, had an Ir–Ir first-shell coordination number of 3.0 ± 0.1 at a distance of 2.67 ± 0.01 Å. The partially decarbonylated tetrairidium clusters chemisorbed hydrogen. Temperature-programmed desorption (TPD) data show that the strength of bonding of hydrogen to the clusters increased with increasing cluster decarbonylation. The completely decarbonylated clusters were characterized by low chemisorption capacities (H/Ir and CO/Ir values, e.g. 0.27 and 0.39, respectively). Chemisorption and EXAFS data show that the amount of hydrogen or CO chemisorbed on Ir_4 increases with increasing size of the iridium clusters and aggregates, consistent with a support effect that is maximized for the smallest clusters, Ir_4. Data representing the catalytic hydrogenation of toluene show that the rate depends on the amount of hydrogen on the clusters — and not just on the degree of decarbonylation — consistent with the suggestion that iridium atoms free of CO ligands are not sufficient for catalysis to proceed. Toluene adsorbed on the support is implicated in the catalysis.

Keywords: Tetrairidium clusters; Toluene hydrogenation; Iridium catalyst

1. Introduction

Supported metal clusters are important catalysts in practice; for example, platinum clusters as small as about 5–10 atoms each, on average, are present in zeolite LTL-supported catalysts for selective dehydrocyclization of naphtha to give aromatics [1,2]. Models of supported metal clusters with nearly uniform structures were prepared by decarbonylation of $[Ir_4(CO)_{12}]$ or $[HIr_4(CO)_{11}]^-$ on various supports [3]. Being simple and nearly uniform in structure, these materials offer opportunities to determine how the cluster nuclearity and the nature of the support influence chemisorption and catalytic properties.

As a part of a continuing investigation [4,5] of supported clusters made from $[Ir_4(CO)_{12}]$ or $[HIr_4(CO)_{11}]^-$, we report a family of MgO-supported iridium catalysts. The goal was to characterize the surface species resulting from various degrees of

* Corresponding author.
[1] Also corresponding author.

1381-1169/00/$ - see front matter
PII: S1381-1169(00)00322-8

decarbonylation of MgO-supported $[HIr_4(CO)_{11}]^-$ and to determine the effect of the carbonyl ligands on chemisorption and catalysis. The work complements that reporting a family of partially decarbonylated clusters formed from $[Ir_4(CO)_{12}]$ on γ-Al_2O_3 [4,5]. Infrared spectroscopy, extended X-ray absorption fine structure (EXAFS) spectroscopy, chemisorption of hydrogen and of CO, temperature-programmed desorption (TPD) of hydrogen, and catalysis of toluene hydrogenation were used to characterize the samples.

2. Experimental

2.1. Materials

$[Ir_4(CO)_{12}]$ (Strem, 98%) was used as supplied. *n*-Pentane solvent (Aldrich, 99%) was refluxed under N_2 in the presence of Na/benzophenone ketyl to remove traces of moisture and deoxygenated by sparging of dry N_2 prior to use. Gases [N_2, He, and H_2 (Matheson, UHP grade)] were purified by flow through traps containing particles of reduced Cu/Al_2O_3 and activated zeolite to remove traces of O_2 and moisture, respectively. The MgO support (MX-65-1 powder, MCB reagents), with a BET surface area of 47 m^2/g (determined by N_2 adsorption), was calcined in O_2 at 400°C for 2 h followed by evacuation at 10^{-3} Torr at 400°C for 14 h.

2.2. Preparation and decarbonylation of MgO-supported $[HIr_4(CO)_{11}]^-$

The catalyst was prepared by contacting $[Ir_4(CO)_{12}]$ with MgO powder in *n*-pentane [4,5]. The synthesis and handling were carried out with air exclusion by use of a Schlenk vacuum line and a N_2-filled drybox. The $[Ir_4(CO)_{12}]$ precursor was used in amounts sufficient to give samples containing 1 wt.% Ir when the uptake by MgO was complete, as was assured by complete removal of the solvent by evacuation. The resultant $[HIr_4(CO)_{11}]^-/MgO$ was decarbonylated in steps by treatment in flowing He or H_2 as the temperature was ramped at the rate of 3°C/min to a temperature within the range of 25–400°C. Decarbonylation was monitored by infrared spectroscopy; the sample was held (typically for 2 h) at a temperature at each step until no further change in the spectrum was observed.

2.3. Infrared spectroscopy

Spectra were recorded with a Bruker IFS-66v spectrometer with a spectral resolution of 4 cm^{-1}. Samples were pressed into self-supporting wafers and mounted in the infrared cell in the drybox. Each sample was scanned 64 times, and the signal was averaged.

2.4. Chemisorption measurements

An RXM-100 multifunctional catalyst testing and characterization system (Advanced Scientific Designs, Inc.) with a vacuum capability of 10^{-8} Torr was used for chemisorption measurements. The sample handling and procedures were as described [5]. Accuracy in values of H/Ir, CO/Ir, and O/Ir ratios was $\pm$10%.

2.5. Temperature-programmed desorption of hydrogen

The RXM-100 system was used for TPD of hydrogen. The sample handling procedures were essentially the same as those used for the chemisorption measurements. Each sample, initially consisting of $[HIr_4(CO)_{11}]^-/MgO$, was partially decarbonylated in He or H_2, evacuated to a pressure of 10^{-5} Torr at the treatment temperature, and then exposed to 200 Torr of H_2 at room temperature for 30 min. After evacuation at room temperature for 0.5 h to remove weakly adsorbed hydrogen, the sample was heated under vacuum as the temperature was ramped from 25 to 400°C at a rate of 10°C/min. Desorbed H_2 was monitored with a quadrupole mass spectrometer (UTI model 100C). The pressure in the system was kept at approximately 4×10^{-5} Torr to minimize readsorption of hydrogen.

2.6. Catalytic hydrogenation of toluene

Details of the sample handling and catalytic hydrogenation of toluene in a flow reactor are as described [5]. Accuracy in the determination of reac-

tion rates (from differential conversions) was about ±10%. Calculations with standard methods showed that the influence of transport phenomena on the reaction rates was negligible.

2.7. EXAFS spectroscopy

EXAFS experiments were performed at X-ray beamline 2–3 at the Stanford Synchrotron Radiation Laboratory (SSRL) at the Stanford Linear Accelerator Center, Stanford, California. The storage ring energy was 3 GeV and the ring current 60–100 mA. EXAFS spectroscopy was used to characterize the surface species formed by adsorption of $[Ir_4(CO)_{12}]$ on MgO as well as the variously decarbonylated samples. Sample handling was as described [4,5].

The EXAFS data were recorded in transmission mode after the cells had been cooled to nearly liquid nitrogen temperature. The data were collected with a Si(2 2 0) double crystal monochromator that was detuned by 20% to minimize effects of higher harmonics in the X-ray beam. The samples were scanned at energies near the Ir L_{III} absorption edge (11215 eV).

3. EXAFS reference data and analysis

The EXAFS data were analyzed with experimentally determined reference files obtained from EXAFS data characterizing materials of known structure, as stated elsewhere [5]. The EXAFS parameters were estimated from the raw data with the aid of the XDAP software [6]. The methods used to extract the EXAFS function from raw data are essentially the same as those reported [5]. Data representing each sample are the average of six scans; the analysis was done with a maximum of 20 free parameters over the range $3.53 < k < 15.69\,\text{Å}^{-1}$ (k is the wave vector) and $0.0 < r < 4.0\,\text{Å}$ (r is the distance from the absorbing atom, Ir). The statistically justified number of free parameters n, was found to be 32, as estimated from the Nyquist theorem [7,8], $n = (2\Delta k\Delta r/\pi) + 1$, where Δk and Δr are the ranges of k and r used in the fitting. The parameters characterizing both Ir-low-Z (O, C) and Ir-high-Z (Ir) contributions were determined by multiple-shell fitting in r space and in k space with application of k^1 and k^3 weighting in the Fourier transformations. The fit was optimized by use of a difference file technique with phase- and amplitude-corrected Fourier transforms. Other details are essentially the same as those reported [4,5].

4. Results

4.1. Infrared evidence of interaction of $[Ir_4(CO)_{12}]$ with MgO

After $[Ir_4(CO)_{12}]$ had been slurried for 14 h with MgO powder in *n*-pentane at 25°C and the solvent removed by evacuation, the color of the solid changed from white to yellow. New bands appeared in the ν_{CO} region of the spectrum of the solid at 2052, 2010, 1970, and 1884 cm^{-1} (Fig. 1, spectrum 1), indicating the formation of the yellow $[HIr_4(CO)_{11}]^-$, as expected [9–12]. Changes in the ν_{OH} and carbon-

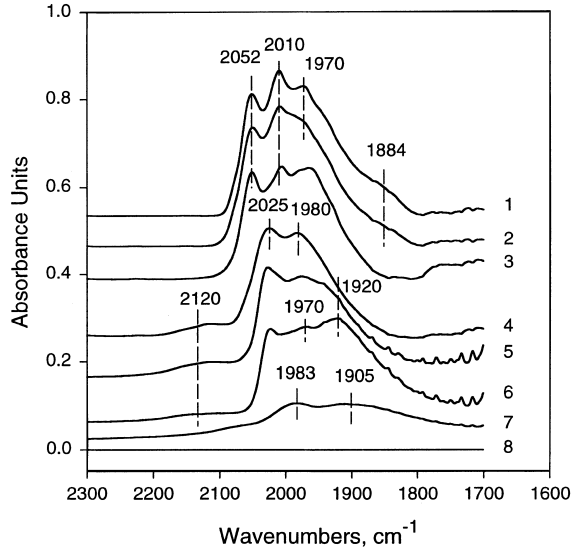

Fig. 1. Infrared spectra in the ν_{CO} region characterizing samples formed from MgO-supported $[HIr_4(CO)_{11}]^-$ after treatment under the following conditions: (1) He at 25°C; (2) H_2 at 25°C; (3) *H_2 at 80°C;* (4) H_2 for 120 min at 100°C; (5) H_2 for 120 min at 150°C; (6) H_2 for 120 min at 200°C; (7) H_2 for 120 min at 300°C; (8) He at 300°C. Note: when the times of contact are not specified, the spectra were independent of time of contact. The treatments printed in italics indicate experiments in which steady state was not attained. In others, steady state was attained.

ate regions of the spectrum were as described earlier [9].

4.2. Infrared evidence of decarbonylation of MgO-supported $[HIr_4(CO)_{11}]^-$ in He

Infrared evidence of the decarbonylation of $[HIr_4(CO)_{11}]^-$/MgO in He has been reported [9]. The ν_{CO} bands representing $[HIr_4(CO)_{11}]^-$ declined in intensity as the temperature increased from 25 to 300°C, and at 300°C, no ν_{CO} bands remained [9]. To estimate the degree of decarbonylation at various temperatures, a sample was held at the desired temperature until no further changes in the spectra were observed, and the remaining areas of the ν_{CO} bands were measured. The areas normalized to the total ν_{CO} area of the untreated $[HIr_4(CO)_{11}]^-$/MgO are summarized in Table 1. Errors in the determination of the ν_{CO} areas were as much as about $\pm 15\%$.

4.3. Infrared evidence of decarbonylation of $[HIr_4(CO)_{11}]^-$/MgO in H_2

Infrared data indicate the decarbonylation of $[HIr_4(CO)_{11}]^-$/MgO in flowing H_2 as the temperature was raised from 25 to 300°C. Small changes in the shapes of the ν_{CO} bands were observed as soon as the sample was exposed to H_2 at 25°C (Fig. 1, spectrum 2). As the temperature increased to 80°C at a rate of 3°C/min (Fig. 1, spectrum 3), the ν_{CO} band at 1884 cm^{-1} disappeared, and the bands at 2052, 2010, and 1970 cm^{-1} declined in intensity (Fig. 1).

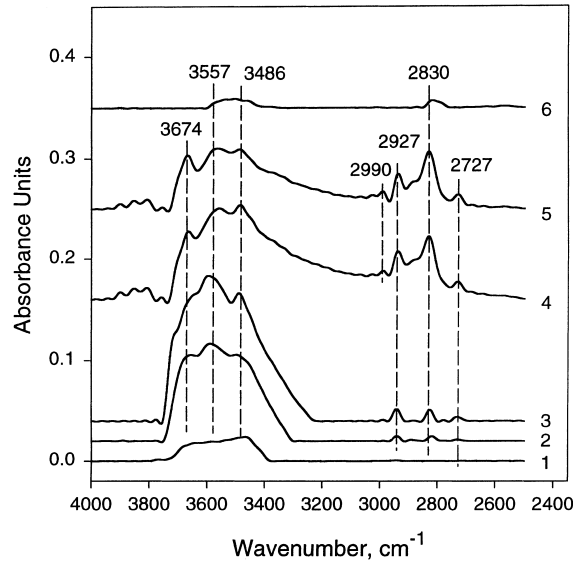

Fig. 2. Infrared spectra in the ν_{OH} and ν_{CH} regions characterizing decarbonylation of $[HIr_4(CO)_{11}]^-$/MgO in H_2 flow under the following conditions: (1) at 25°C; (2) *after 5 min at 80°C;* (3) after 120 min at 100°C; (4) after 120 min at 150°C; (5) after 120 min at 200°C; (6) after 120 min at 300°C. Also see the note in the caption of Fig. 1.

The changes in area of the ν_{CO} peaks indicate that about 18% of the CO ligands were removed by the treatment. When the temperature was raised further to 100°C, the spectrum changed markedly; the ν_{CO} bands at 2052, 2010, and 1970 cm^{-1} were no longer evident, and new bands appeared at 2120, 2025, and 1980 cm^{-1} (Fig. 1, spectrum 4). A subsequent in-

Table 1
Hydrogen chemisorption capacity and catalytic activity for toluene hydrogenation of MgO-supported iridium clusters formed from $[HIr_4(CO)_{11}]^-$ and decarbonylated to various degrees by treatment in flowing He

Treatment gas	Temperature (°C)	Percentage of CO ligands left in supported iridium carbonyl cluster[a]	Chemisorption at 25°C, atomic ratio (H/Ir)	Catalytic activity[b] (mol MCH/mol Ir · s)	TOF (s^{-1})[c]	Apparent activation energy, E_a (kcal/mol)
None	–	100	0.00	0.0	–	–
He	100	57.8	0.02	2.87×10^{-6}	6.80×10^{-6}	4.7
He	150	33.9	0.07	3.72×10^{-6}	5.63×10^{-6}	9.2
He	200	13.2	0.10	4.99×10^{-6}	5.75×10^{-6}	9.6
He	250	3.9	0.16	3.52×10^{-5}	3.66×10^{-5}	10.6
He	300	0.0	0.27	3.24×10^{-4}	3.25×10^{-4}	13.1

[a] Determined on the basis of infrared peak areas.
[b] Reaction at 60°C, $P_{toluene} = 50$ Torr, and $P_{H_2} = 710$ Torr. MCH is methylcyclohexane.
[c] Turnover frequency is represented here as reaction rate per iridium atom without CO ligands estimated from the infrared peak areas.

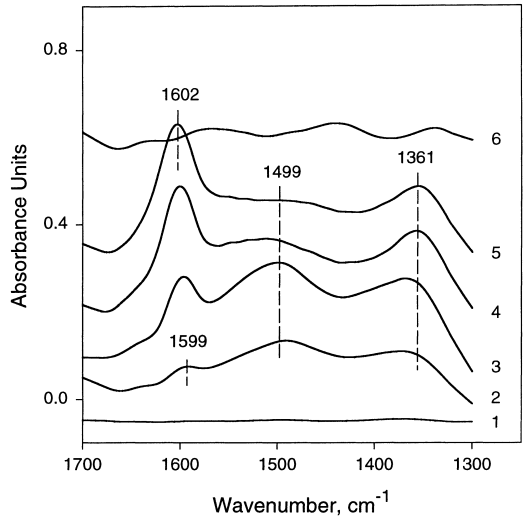

Fig. 3. Infrared spectra in the ν_{COO} region characterizing decarbonylation of MgO-supported $[HIr_4(CO)_{11}]^-$ in H_2 flow under the following conditions: (1) at 25°C; (2) after 5 min at 80°C; (3) after 120 min at 100°C; (4) after 120 min at 150°C; (5) after 120 min at 200°C; (6) after 120 min at 300°C.

crease in the temperature to 200°C led to splitting and broadening of these bands without substantial changes in the areas (Fig. 1, spectra 5–6). As the temperature increased to 300°C, the spectrum changed markedly again, with two broad bands remaining at 1983 and 1905 cm^{-1} (Fig. 1, spectrum 7); these bands were always present when the sample was exposed to H_2 at 300°C, but they were readily removed by treatment in He at 300°C (Fig. 1, spectrum 8).

The decarbonylation of $[HIr_4(CO)_{11}]^-/MgO$ in H_2 was accompanied by changes in the ν_{OH}, ν_{CH}, and ν_{COO} regions of the spectrum (Figs. 2 and 3). The flow of H_2 through the sample at room temperature led to increasing absorption in the range of 3674–3486 cm^{-1}, associated with hydrogen-bonded OH groups of MgO (Fig. 2, spectrum 1). The intensity of the OH bands increased substantially as the temperature increased, and new bands were observed in the ν_{CH} and ν_{COO} regions, at 2990, 2927, 2830, 2727, 1599, 1499, and 1361 cm^{-1}. The bands at 2830 and 2727 cm^{-1} are assigned to the symmetric and asymmetric C–H stretching frequencies of surface formate, respectively, and those at 1599 and 1361 cm^{-1} to asymmetric and symmetric ν_{COO} of surface formate, respectively [13]. The bands at 2990 and 2927 cm^{-1} might be attributed to ν_{CH} of hydrocarbons and that at 1499 cm^{-1} to the asymmetric C–O stretching vibration of free CO_3^{2-} ions on MgO.

Table 2
Dispersions, chemisorption capacities, and catalytic activities for toluene hydrogenation of MgO-supported iridium clusters and aggregates formed from $[HIr_4(CO)_{11}]^-$ by treatment in He or H_2 flowing at various temperatures

Treatment gas	Treatment temperature (°C)	Chemisorption capacity at 25°C, atomic ratio[a]			N^b_{Ir-Ir}	D (Å)[c]	Ir_s/Ir_t[d]	TOF (s^{-1})[e]	Apparent activation energy, E_a (kcal/mol)
		H/Ir	CO/Ir	O/Ir					
He	300	0.27	0.39	1.51	3.0	5.6	1.0	3.2×10^{-4}	13.1
He	400	1.00	0.72	1.57	4.0	7.6	1.0	4.7×10^{-4}	10.8
H_2	300	1.10	0.93	1.55	6.7	11.6	0.81	9.2×10^{-4}	10.5
H_2	400	1.28	0.87	1.25	7.7	14.5	0.70	13.1×10^{-3}	14.6
H_2	400								
followed by									
O_2	300								
and then									
H_2	400	1.36	0.79	1.12	10.6	~35.0	~0.32	29.2×10^{-3}	13.4

[a] For CO adsorption, the data represent the number of molecules of CO per Pt atom.
[b] First-shell Ir–Ir coordination number estimated on the basis of EXAFS data; see text.
[c] Diameter of metal clusters determined from EXAFS data on the basis of calculations reported by Kip et al. [34].
[d] Calculated dispersion expressed as the ratio of the number of surface iridium atoms to total number of iridium atoms in the clusters or aggregates.
[e] Reaction conditions as in Table 1. The turnover frequency is represented here as the reaction rate normalized by the fraction of surface iridium atoms.

4.4. Chemisorption of H_2 on partially decarbonylated iridium clusters

After $[HIr_4(CO)_{11}]^-$/MgO had been partially decarbonylated by treatment in He at various temperatures, the resultant surface species were able to adsorb hydrogen. The data (Table 1) show the dependence of the H/Ir values on the degree of decarbonylation.

4.5. Chemisorption of hydrogen, CO, and oxygen on fully decarbonylated iridium clusters and aggregates

The H/Ir, CO/Ir, and O/Ir values representing the amounts of hydrogen, CO, or oxygen irreversibly chemisorbed on the completely decarbonylated iridium clusters are summarized in Table 2. The H/Ir and CO/Ir values characterizing the clusters formed by decarbonylation of $[HIr_4(CO)_{11}]^-$/MgO in He at 300°C (Table 2) agree well with previous reports [9] but are markedly less than those observed for conventionally prepared supported iridium catalysts, prepared from salt precursors by calcination and reduction in H_2 [14]. The O_2 chemisorption results (Table 2) indicate an O/Ir ratio of about 1.5 at 25°C, demonstrating the formation of Ir_2O_3. The data of Fig. 4 clearly indicate a strong dependence of H/Ir and CO/Ir values on the iridium cluster or aggregate size.

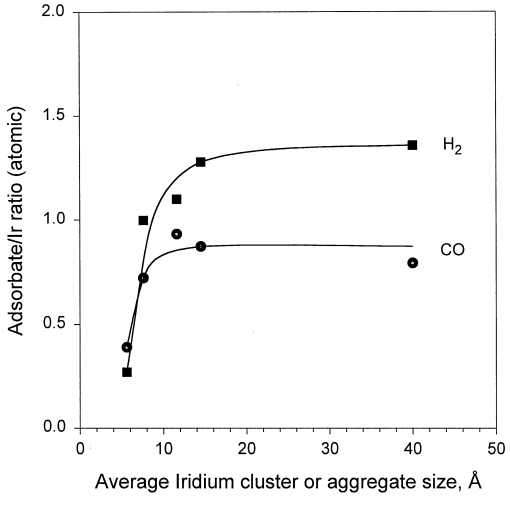

Fig. 4. Dependence of hydrogen and CO chemisorption capacities on the average iridium cluster or aggregate size.

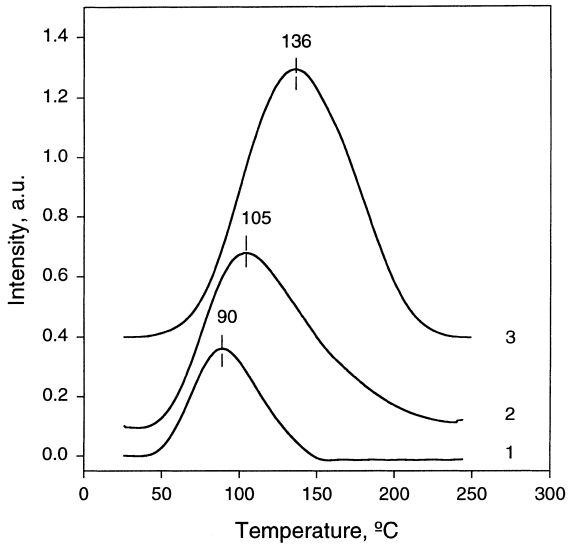

Fig. 5. TPD profiles of hydrogen preadsorbed at monolayer coverage on samples formed from $[HIr_4(CO)_{11}]^-$/MgO that had been decarbonylated to various degrees in He at the following temperatures (°C): (1) 150; (2) 250; (3) 300.

4.6. TPD data

Fig. 5 represents profiles of H_2 desorbing from partially decarbonylated supported clusters. When hydrogen was adsorbed on the sample decarbonylated in He at 150°C, on which about 34% of the initial CO ligands remained (as estimated from the infrared data), a single peak with a maximum at 90°C was observed (Fig. 5). Further decarbonylation led not only to increasing TPD peak intensity, but also to shifting of the peak maximum to higher temperatures. The maximum desorption rate of H_2 (from the completely decarbonylated sample) was observed at about 136°C (Fig. 5).

Fig. 6 represents profiles of hydrogen desorbing from samples that had been decarbonylated under various conditions. When $[HIr_4(CO)_{11}]^-$/MgO had been completely decarbonylated by treatment in H_2 at 300°C, the position of the desorption peak was the same as that observed for the sample decarbonylated in He, but its intensity was higher (Fig. 6, spectra 1 and 2). Increasing the temperature of decarbonylation in H_2 led to substantial changes in the shapes of the TPD profiles. A new peak with a maximum at 188°C indicated an additional hydrogen species (Fig.

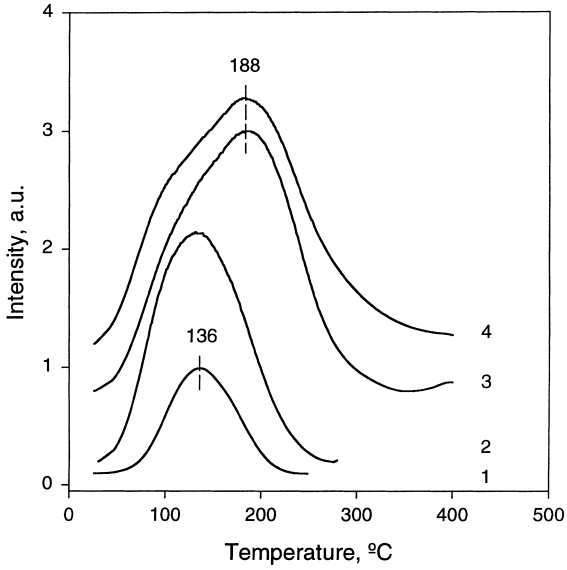

Fig. 6. TPD profiles of hydrogen preadsorbed at monolayer coverage on samples formed from $[HIr_4(CO)_{11}]^-$/MgO that had been decarbonylated at the following conditions: (1) in He at 300°C; (2) in H_2 at 300°C; (3) in H_2 at 400°C; (4) in H_2 at 400°C followed by O_2 at 300°C and then H_2 at 400°C.

6, spectrum 3); the peak at 136°C was evident as a shoulder (Fig. 6, spectra 3 and 4).

4.7. EXAFS data characterizing MgO-supported iridium clusters and aggregates

The parameters obtained in the data fitting for the samples treated in He or H_2 at various temperatures are summarized in Tables 3 and 4, respectively. The XDAP software [6] was used to estimate error bounds in the parameters reported in Tables 3 and 4, which represent precisions determined from statistical analysis of the data, not accuracies. Estimated accuracies are as follows: coordination number (N), $\pm 20\%$; distance (R) between absorber (Ir) and backscatterer atoms, $\pm 1\%$; Debye–Waller factor ($\Delta\sigma^2$), $\pm 30\%$; inner potential correction (ΔE_0), $\pm 10\%$.

The Ir–Ir first-shell coordination numbers (each 3.0 ± 0.1) show that the tetrahedral metal frames of the clusters treated in He at temperatures up to 300°C remained intact throughout the decarbonylation (Table 3). In contrast, treatment in H_2 led to aggregation of the iridium (the higher the temperature of treatment, the larger the aggregates that were formed), as shown by the changes in the first-shell Ir–Ir coordination numbers (Table 4).

4.8. Catalysis of toluene hydrogenation

The catalytic results characterizing partially decarbonylated supported iridium clusters and those characterizing the completely decarbonylated clusters and aggregates are summarized in Tables 1 and 2, respectively. Fig. 7 illustrates the dependence of the catalytic reaction rate on the percentage of CO ligands removed from the clusters. Each reaction rate corresponds to 2 h on stream, corresponding to virtually a steady-state operation. Turnover frequencies (TOF) characterizing partially decarbonylated clusters (Table 1) were determined from reaction rates normalized to the number of iridium atoms free of CO ligands, as described elsewhere [5]. TOF values characterizing completely decarbonylated clusters (Table 2) were calculated on the basis of the assumption that each iridium atom was accessible, and any blockage by the support was ignored. Values representing the aggregated iridium (Table 2) were calculated per exposed iridium atom estimated by taking into account the iridium dispersion determined from the EXAFS Ir–Ir first-shell coordination numbers, as reported elsewhere [4,15] (again, any blockage by the support was ignored). Values of the apparent activation energy (Tables 1 and 2) calculated from the temperature dependencies of the reaction rates were found to be similar to those reported earlier for γ-Al_2O_3-supported iridium samples [4,5,16].

5. Discussion

5.1. Formation of $[HIr_4(CO)_{11}]^-$ on MgO

Similar to the chemistry of $[Ir_4(CO)_{12}]$ in basic solutions [17], the chemistry of $[Ir_4(CO)_{12}]$ on the surfaces of basic oxides leads to the formation of carbonyliridate anions with compositions that depend on the basicity of the support [18–20]. The interaction of $[Ir_4(CO)_{12}]$ with partially dehydroxylated MgO (treated under vacuum at 400°C) leads to the formation of $[HIr_4(CO)_{11}]^-$, presumably as a result of nucleophilic attack of surface OH groups on

Table 3
EXAFS results at the Ir L_{III} edge characterizing the supported species formed by decarbonylation of $[HIr_4(CO)_{11}]^-$ on MgO in He at various temperatures[a]

Temperature of treatment (°C)	Shell	Ir–Ir contribution				$Ir–O_{support}$ ($Ir–O_s^b$ and $Ir–O_l^c$) contributions				Ir–CO terminal ($Ir–C^d$ and $Ir–O^{*e}$) and bridging ($Ir–C^f$ and $Ir–O^{*g}$) contributions			
		N	R (Å)	$10^3 \times \Delta\sigma^2$ (Å^2)	ΔE_0 (eV)	N	R (Å)	$10^3 \times \Delta\sigma^2$ (Å^2)	ΔE_0 (eV)	N	R (Å)	$10^3 \times \Delta\sigma^2$ (Å^2)	ΔE_0 (eV)
No treatment	First	3.0 ± 0.1	2.70 ± 0.01	3.4 ± 0.2	4.9 ± 0.4	–	–	–	–	2.1 ± 0.1^d	1.84 ± 0.01	3.3 ± 0.3	3.0 ± 0.5
										2.2 ± 0.1^e	2.93 ± 0.01	1.0 ± 0.4	5.1 ± 0.3
										0.8 ± 0.1^f	2.05 ± 0.01	-0.6 ± 0.7	3.3 ± 0.6
										0.9 ± 0.1^g	3.31 ± 0.01	2.8 ± 0.6	7.9 ± 0.4
100 for 2 h	First	3.0 ± 0.1	2.68 ± 0.01	2.1 ± 0.3	-0.2 ± 0.3	0.8 ± 0.1^b	2.12 ± 0.01	-2.0 ± 0.4	-7.1 ± 0.3	0.5 ± 0.1^d	1.83 ± 0.01	-3.9 ± 0.3	-4.0 ± 0.9
						1.1 ± 0.1^c	2.78 ± 0.01	-0.6 ± 0.5	-5.1 ± 0.3	0.8 ± 0.1^e	2.96 ± 0.01	-5.1 ± 0.2	-3.5 ± 0.2
200 for 2 h	First	3.1 ± 0.1	2.68 ± 0.01	2.6 ± 0.2	-0.2 ± 0.1	0.7 ± 0.1^b	2.11 ± 0.01	0.1 ± 0.4	-8.0 ± 0.4	0.2 ± 0.1^d	1.80 ± 0.01	-8.1 ± 0.2	-13.0 ± 0.8
						1.5 ± 0.1^c	2.73 ± 0.01	3.4 ± 0.4	0.0 ± 0.2	0.5 ± 0.1^e	2.98 ± 0.01	-5.2 ± 0.1	-10.2 ± 0.2
300 for 2 h	First	3.0 ± 0.1	2.67 ± 0.01	5.5 ± 0.2	-0.7 ± 0.3	1.0 ± 0.1^b	2.19 ± 0.01	10.0 ± 0.7	-15.4 ± 0.6	–	–	–	–
						0.9 ± 0.1^c	2.68 ± 0.01	-1.9 ± 0.3	-5.2 ± 0.4	–	–	–	–
400 for 2 h	First	4.0 ± 0.1	2.67 ± 0.01	3.9 ± 0.2	-3.7 ± 0.3	0.9 ± 0.1^b	2.17 ± 0.02	8.4 ± 1.6	-14.0 ± 0.7	–	–	–	–
						1.0 ± 0.1^c	2.66 ± 0.01	0.3 ± 0.8	-4.0 ± 0.3	–	–	–	–
	Second	1.4 ± 0.2	3.79 ± 0.01	6.0 ± 1.2	-2.0 ± 0.6	–	–	–	–	–	–	–	–

[a] Notation: N, coordination number; R, distance between absorber and backscatterer atoms; $\Delta\sigma^2$, Debye–Waller factor; ΔE_0, inner potential correction; the subscripts s and l refer to short and long, respectively.

Table 4
EXAFS results at the Ir L_{III} edge characterizing the surface species formed by decarbonylation of $[HIr_4(CO)_{11}]^-$ on MgO in H_2 at various temperatures[a]

Treatment conditions (°C)	Shell	Ir–Ir contribution				Ir–O support ($Ir–O_s^b$ and $Ir–O_l^c$) contributions				Ir–CO ($Ir–C^d$ and $Ir–O^{*e}$) contributions			
		N	R (Å)	$10^3 \times \Delta\sigma^2$ (Å^2)	ΔE_0 (eV)	N	R (Å)	$10^3 \times \Delta\sigma^2$ (Å^2)	ΔE_0 (eV)	N	R (Å)	$10^3 \times \Delta\sigma^2$ (Å^2)	ΔE_0 (eV)
100 for 2 h	First	3.0 ± 0.1	2.71 ± 0.01	5.3 ± 0.4	11.9 ± 0.6	0.6 ± 0.1[b]	2.18 ± 0.01	10.0 ± 1.6	−19.9 ± 1.9	1.0 ± 0.1[d]	1.82 ± 0.01	−0.4 ± 0.4	4.0 ± 1.4
										1.7 ± 0.1[e]	2.92 ± 0.01	0.9 ± 0.4	3.9 ± 0.3
200 for 2 h	First	3.0 ± 0.1	2.70 ± 0.01	2.4 ± 0.2	12.1 ± 0.2	0.6 ± 0.1[b]	2.22 ± 0.01	6.5 ± 2.1	−19.5 ± 1.9	0.5 ± 0.1[d]	1.84 ± 0.01	−2.1 ± 0.3	−3.1 ± 1.7
						2.4 ± 0.2[c]	2.70 ± 0.01	10.0 ± 1.1	−2.8 ± 0.8	0.2 ± 0.1[e]	2.98 ± 0.01	−6.4 ± 0.2	−2.6 ± 0.3
250 for 2 h	First	3.0 ± 0.1	2.69 ± 0.01	3.4 ± 0.2	8.7 ± 0.6	0.4 ± 0.1[b]	2.24 ± 0.01	−1.4 ± 0.5	−19.5 ± 0.8	0.2 ± 0.1[e]	1.78 ± 0.01	−4.1 ± 0.6	3.0 ± 2.6
						2.7 ± 0.1[c]	2.72 ± 0.01	10.0 ± 0.5	−5.9 ± 0.6	–	–	–	–
300 for 2 h	First	6.7 ± 0.2	2.68 ± 0.01	4.7 ± 0.1	2.0 ± 0.2	0.6 ± 0.1[b]	2.18 ± 0.01	3.2 ± 1.2	−9.9 ± 0.9	–	–	–	–
						1.2 ± 0.1[c]	2.83 ± 0.01	0.9 ± 0.7	−15.0 ± 0.8	–	–	–	–
	Second	2.5 ± 0.3	3.81 ± 0.01	7.0 ± 0.8	−2.0 ± 0.8	–	–	–	–	–	–	–	–
400 for 2 h	First	7.7 ± 0.1	2.68 ± 0.01	4.6 ± 0.1	1.4 ± 0.2	0.6 ± 0.1[b]	2.14 ± 0.01	10.0 ± 2.5	−5.8 ± 1.8	–	–	–	–
						1.0 ± 0.1[c]	2.79 ± 0.01	−4.1 ± 0.2	−11.0 ± 0.3	–	–	–	–
	Second	3.6 ± 0.2	3.80 ± 0.01	6.5 ± 0.5	1.5 ± 0.6	–	–	–	–	–	–	–	–
H_2 at 400 for 2 h followed by O_2 at 300 for 1 h and then H_2 at 400 for 2 h	First	10.6 ± 0.1	2.68 ± 0.01	5.6 ± 0.1	−0.9 ± 0.2	1.0 ± 0.1[b]	2.10 ± 0.01	10.0 ± 1.1	0.0 ± 0.9	–	–	–	–
						0.4 ± 0.1[c]	2.76 ± 0.01	−10.0 ± 0.1	−12.3 ± 0.2	–	–	–	–
	Second	7.1 ± 0.3	3.80 ± 0.01	10.0 ± 0.3	−1.6 ± 0.3	–	–	–	–	–	–	–	–
	Third	3.6 ± 0.1	4.65 ± 0.01	3.0 ± 0.2	2.0 ± 0.3	–	–	–	–	–	–	–	–

[a] Notation as in Table 3.

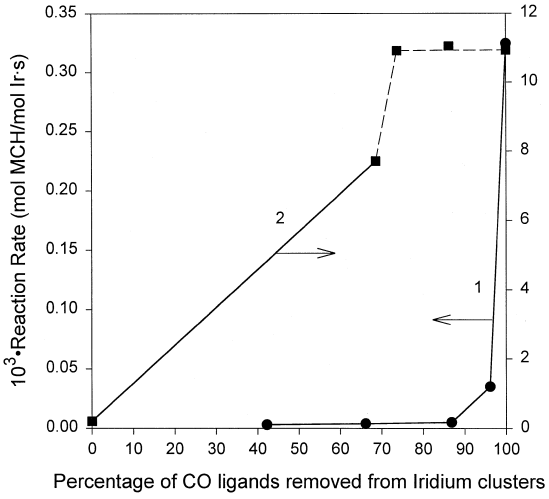

Fig. 7. Toluene hydrogenation catalyzed by partially decarbonylated $[HIr_4(CO)_{11}]^-$ clusters supported on MgO (1) and by partially decarbonylated $[Ir_4(CO)_{12}]$ on γ-Al_2O_3 (2) [9]: dependence of the reaction rate on the degree of decarbonylation of the supported clusters.

terminal CO ligands bonded to iridium [9]. Such cluster-surface interactions have been suggested to lead to the removal of one of the terminal CO ligands from $[Ir_4(CO)_{12}]$, to the formation of two bridging CO ligands as a result of rearrangement of the remaining terminal CO ligands, and to the formation of a hydride ligand, which in the cluster in the crystalline state is a bridging hydride [21]. Since the negative charge of $[HIr_4(CO)_{11}]^-$ is predominantly associated with the iridium atoms [21], the bonding of CO to the electron-rich iridium results in increased electron transfer from filled iridium d-orbitals to the CO $2\pi^*$ antibonding molecular orbitals. As a result, the formation of $[HIr_4(CO)_{11}]^-$ is characterized by the shifting of the terminal ν_{CO} bands representative of $[Ir_4(CO)_{12}]$ (2112, 2072, 2062, 2029, and 2002 cm^{-1}) to lower frequencies. Therefore, the infrared spectrum (with bands at 2052, 2010, 1970, and 1884 cm^{-1}) observed upon interaction of $[Ir_4(CO)_{12}]$ with MgO (Fig. 1, spectrum 1) is almost the same as those reported [11,12,18] for MgO-supported $[HIr_4(CO)_{11}]^-$ identified by infrared spectra of the cluster anions extracted from the surface with bis(triphenylphosphine)iminium chloride [12].

The EXAFS data summarized in Tables 3 and 5 provide strong structural evidence confirming the presence of $[HIr_4(CO)_{11}]^-$ formed from $[Ir_4(CO)_{12}]$ on MgO. The crystallographic parameters determined for $[Ir_4(CO)_{11}]^-$ by X-ray [19] and neutron [21] diffraction show that the four iridium atoms are arranged in a regular tetrahedron with an Ir–Ir distance of 2.73 Å. The iridium atom located at the apex of the tetrahedron has three terminal CO ligands, with Ir–C_t (t is terminal) and Ir–O_t^* (O^* is carbonyl oxygen) contributions at average distances of 1.84 and 2.99 Å, respectively; each iridium atom located at the basal plane is bonded to two terminal CO ligands and participates in bonding of two bridging CO ligands, with Ir–C_b (b is bridging) contributions observed at an average distance of 2.08 Å. The Ir L_{III}-edge EXAFS results characterizing the sample formed from $[Ir_4(CO)_{12}]$ on MgO agree well with these structural data, including an Ir–Ir contribution with a coordination number of 3.0 at a distance of 2.70 Å (Tables 3 and 5), as well as terminal and bridging carbonyls, with Ir–C_t and Ir–C_b coordination numbers of 2.1 and 0.8 at distances of 1.84 and 2.05 Å, respectively. The Ir–O_t^* and Ir–O_b^* contributions are represented by coordination numbers of 2.2 and 0.9 and bond distances of 2.93 and 3.31 Å, respectively (Tables 3 and 5). Within the expected experimental uncertainty, the EXAFS results for the MgO-supported iridium carbonyl match the crystallographic data for $[HIr_4(CO)_{11}]^-$, as expected [12].

Table 5
Comparison of crystallographic data for $[HIr_4(CO)_{11}]^-$ [21] and EXAFS results for MgO-supported sample prepared from $[Ir_4(CO)_{12}]$[a]

Contribution	Crystallographic data for $[HIr_4(CO)_{11}]^-$			EXAFS	
	N	Neutron diffraction	XRD	N	R (Å)
		R (Å)	R (Å)		
Ir–Ir	3.0	2.74	2.73	3.0	2.70
Ir–C_t	2.3	1.89	1.84	2.1	1.84
Ir–O_t^*	2.3	3.04	2.99	2.2	2.93
Ir–C_b	1.0	2.09	2.08	0.8	2.05
Ir–O_b^*	1.0	–	–	0.9	3.31

[a] Notation as in Table 3.

5.2. Formation of partially decarbonylated tetrairidium clusters on MgO by treatment in He

Infrared data [9] indicate that MgO-supported $[HIr_4(CO)_{11}]^-$ was completely decarbonylated by treatment in He at 300°C. Consistent with these data, the Ir L_{III}-edge EXAFS data (Table 3) show that Ir–C and Ir–O* contributions associated with CO ligands gradually became smaller as the treatment temperature increased to 200°C, indicating cluster decarbonylation. After treatment at 300°C, there was no EXAFS evidence of any remaining Ir–CO contributions (Table 3), consistent with the infrared data [9]. Before the MgO-supported clusters were decarbonylated, there were no $Ir–O_{support}$ contributions in the EXAFS spectra (Table 3), consistent with the inference that the Ir_4 core of a fully carbonylated cluster was not in close contact with the support. As some of the CO ligands were removed by treatment in He at 100°C, there was greater contact between the cluster core and the support, as shown by the appearance of two $Ir–O_{support}$ contributions, at distances of 2.12 and 2.78 Å. Similar $Ir–O_{support}$ contributions were reported for iridium clusters on MgO [22,23] and on γ-Al_2O_3 [4,5,24,25], as discussed elsewhere [22,23].

The result that the first-shell Ir–Ir coordination number was about 3.0 throughout the decarbonylation process at temperatures up to 300°C (Table 3) shows that the tetrahedral cluster frame was stable throughout the decarbonylation process. However, after treatment in He at 400°C, the sample was characterized by a larger Ir–Ir first-shell coordination number (4.0) and by a new second-shell Ir–Ir contribution (with a coordination number of 1.4 at a distance of 3.79 Å). Thus, the iridium had aggregated slightly; the data indicate an increasing mobility of MgO-supported iridium in He at the higher temperatures, as was observed for γ-Al_2O_3-supported iridium [4].

5.3. Formation of partially decarbonylated and aggregated iridium clusters by treatment of $[HIr_4(CO)_{11}]^-$/MgO in H_2

The infrared data of Figs. 1–3 indicate that decarbonylation of $[HIr_4(CO)_{11}]^-$/MgO in the presence of H_2 is more complicated than that in the presence of He [9]. The ν_{CO} bands (2052, 2010, and 1970 cm^{-1}) were clearly evident in the spectra only at temperatures up to 80°C (Fig. 1), and at 100°C new bands appeared, at 2120, 2025, and 1980 cm^{-1}. The frequency of the weak band at 2120 cm^{-1} is too high to be attributed to the ν_{CO} associated with MgO-supported iridium. The positions of these new bands are very similar to those of the Ir–H stretching vibrations (2120, 2020, and 1980 cm^{-1}) observed after exposure of iridium supported on Al_2O_3 to H_2 [26,27], and so we tentatively attribute the bands to iridium hydrides. When the temperature of H_2 treatment increased to 200°C, the areas of these peaks remained unchanged (Fig. 1), contrary to the decline in intensity that would be expected for iridium carbonyls. However, we cannot exclude the possibility that some CO bands were still present in the infrared spectra in the range of 1800–2100 cm^{-1}, but possible overlapping ν_{CO} and ν_{IrH} bands are not resolved, and we lack the basis for estimating how much CO remained in the samples; the EXAFS data show that some CO remained bonded to the clusters after H_2 treatment at 200°C (Table 4).

After H_2 treatment at 300°C, the sample was completely decarbonylated, as shown by the EXAFS data (Table 4). The intensities of the infrared bands attributed to the iridium hydrides declined as the treatment temperature increased to 300°C, consistent with removal of hydrogen from the iridium (Fig. 7, spectrum 7). The Ir–H species were easily removed by treatment in He at 300°C (Fig. 1, spectrum 8), but they were found to be stable with the sample in H_2 at 1 atm at this temperature, as evidenced by the two broad bands at 1983 and 1905 cm^{-1} (Fig. 1, spectrum 7).

The infrared data of Figs. 2 and 3 provide additional insight into the chemistry of the decarbonylation in H_2, indicating that CO removed from the cluster interacts with the basic MgO support surface, resulting in the formation of formate (evidenced by ν_{CH} at 2830 and 2727 cm^{-1} and by ν_{COO} at 1599 and 1361 cm^{-1}) and carbonate (evidenced by ν_{CO} at 1499 cm^{-1}), the characteristic bands of which increased in intensity as the temperature increased (and the degree of decarbonylation increased). The data (Fig. 2) also provide evidence that CO ligands participate in reactions with H_2, resulting in the formation

of water and possibly of hydrocarbons, as evidenced by the increased absorption in the ν_{OH} region and by the appearance of bands at 2990 and 2927 cm^{-1} typical of ν_{CH} of hydrocarbons. Thus, we infer that C–O bond-breaking reactions occurred and that the surface chemistry bears some resemblance to that of Fisher–Tropsch catalysis [28].

The EXAFS data show that decarbonylation of $[HIr_4(CO)_{11}]^-/MgO$ in H_2 led to aggregation of the iridium. For example, the first-shell Ir–Ir coordination number was found to be 3.0 after H_2 treatment at 100–250°C, indicating that the frame of the supported clusters was nearly Ir_4 (Table 4). After treatment at 300°C, however, a first-shell Ir–Ir coordination number had increased to 6.7, and a second-shell Ir–Ir contribution with an average coordination number of 2.5 (at a distance of 3.81 Å) was also observed (Table 4). These data indicate the formation of iridium aggregates with average diameters of about 12 Å. Further increases in temperature led to larger iridium aggregates. The increased aggregation of iridium could be related to increased hydroxylation of the support surface (a result of the reaction between H_2 and the iridium carbonyl clusters, as shown by the infrared data), which is known to facilitate migration of supported iridium [18–20]. Thus, as for decarbonylation of $[Ir_4(CO)_{12}]/\gamma\text{-}Al_2O_3$ [4], decarbonylation of $[HIr_4(CO)_{11}]^-/MgO$ in H_2 leads to markedly more rapid aggregation of iridium than that occurring in the presence of He.

5.4. Chemisorption of hydrogen on partially decarbonylated iridium clusters

Consistent with the data characterizing $[Ir_4(CO)_{12}]/\gamma\text{-}Al_2O_3$ [5], no hydrogen chemisorption was observed on $[HIr_4(CO)_{11}]^-/MgO$ (Table 1). This result is expected, because $[HIr_4(CO)_{11}]^-$ is coordinatively saturated, and, in the absence of decarbonylation, lacks open iridium sites for bonding of hydrogen.

As the $[HIr_4(CO)_{11}]^-/MgO$ was gradually decarbonylated, the amount of hydrogen that could be chemisorbed increased, as evidenced by the chemisorption and TPD data (Table 1and Fig. 5). The chemisorption data indicate that the H/Ir values depend in a nonlinear fashion on the amount of CO removed from the clusters (Fig. 8). These data imply

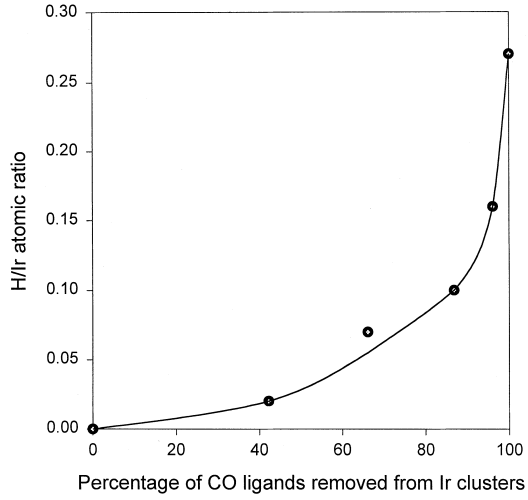

Fig. 8. Dependence of the H/Ir atomic ratio on the degree of decarbonylation of the MgO-supported $[HIr_4(CO)_{11}]^-$ clusters.

that not all the iridium atoms that had lost CO ligands offered bonding sites for hydrogen. TPD profiles characterizing the desorption of hydrogen from the clusters that were decarbonylated to various degrees (Fig. 5) show that the position of the TPD peak maximum shifted to higher temperatures with increasing decarbonylation and increasing coverage by hydrogen. The spectra representing TPD of hydrogen from supported metals show that the maximum desorption rate is observed at lower temperatures with increasing initial surface coverage by hydrogen [15,29–32]. The trend observed in our data is different from that typically found for hydrogen desorption from supported metal particles, consistent with the suggestion that when MgO-supported iridium clusters are not ligand-free, the iridium atoms in the clusters behave differently from those in metallic particles.

Thus, the TPD (Fig. 5) and hydrogen chemisorption data (Table 1) might be explained on the basis of the electronic state of the iridium in partially decarbonylated clusters. The coordinatively saturated $[HIr_4(CO)_{11}]^-$ bears a negative charge [21]. The XANES region of the X-ray absorption data [23] indicates that the fully decarbonylated MgO-supported iridium clusters modeled as Ir_4 have electron densities similar to that of iridium in crystalline $[Ir_4(CO)_{12}]$. Thus, we might suggest that the electron density on iridium would decrease with decreasing

numbers of carbonyl ligands on the cluster. The dissociative chemisorption of H_2 on the iridium clusters would be expected to proceed by donation of electron density from hydrogen to iridium, and the amount of hydrogen chemisorbed might be reduced when the iridium atoms are negatively charged. Thus, some of the iridium atoms freed of carbonyls might not interact strongly with hydrogen atoms because of their electronic environments. These suggestions might explain (at least in part) the nonlinear dependence of H/Ir on the degree of cluster decarbonylation.

Moreover, the TPD data showing a dependence of the temperature of the hydrogen TPD peak maximum on the degree of cluster decarbonylation (Fig. 5) are consistent with the suggestion that the strength of interaction of hydrogen with the iridium is maximized when the excess of electron density on iridium is minimized; in other words, the TPD data indicate that the higher the degree of cluster decarbonylation, the more strongly the hydrogen species are bonded to the iridium. The existence of various forms of hydrogen that differ from each other in the strength of interaction with iridium could affect the H/Ir values determined for the partially decarbonylated clusters (Table 1); clusters with a low degree of decarbonylation are suggested to have mainly weakly bonded hydrogen species, and a substantial fraction of these might be removed during the evacuation step in the chemisorption experiments. Such unaccounted for desorption could result in an underestimation of the H/Ir values for the partially decarbonylated clusters.

5.5. Chemisorption properties of fully decarbonylated iridium clusters and aggregates

The H/Ir and CO/Ir values characterizing the supported species made by decarbonylation of $[HIr_4(CO)_{11}]^-$/MgO in He at 300°C (and modeled as Ir_4) were found to be 0.27 and 0.39, respectively (Table 2), in good agreement with previous reports [9]. In view of the fact that all the iridium atoms in the decarbonylated clusters were available for oxygen chemisorption (as evidenced by the formation of Ir_2O_3 at room temperature), the data of Table 2 indicate reduced H_2 and CO chemisorption on the most highly dispersed iridium clusters. Possible explanations of these results include blockage of access to the iridium, either by the support or by carbon formed during decarbonylation, and/or an electronic effect of the support affecting the reactivity of the clusters [5,9]. Theoretical results at the density functional level [33] show that metal–$O_{surface}$ bonds are strong and that the support should be regarded as a multidentate ligand. More data are needed to resolve the issues.

The data of Table 2 show how the amount of hydrogen or CO chemisorbed on iridium depends on the cluster or aggregate size. A sharp increase in the H/Ir and CO/Ir values was observed when the average cluster or aggregate size increased from about 6 to about 12 Å (Fig. 4), but for larger aggregates, the H/Ir and CO/Ir values do not depend significantly on the size, consistent with the expectation that the support effect decreases as the clusters or aggregates become larger so that a smaller fraction of the iridium atoms are in contact with the support. The H/Ir ratio was found to be 1.0 for clusters of about 8 Å in average diameter and greater than 1 for larger clusters and aggregates (Table 2). The fact that the H/Ir values exceed 1 is consistent with reports of values about 2–2.5 for larger iridium particles on Al_2O_3, consistent with the ability of an iridium atom in a surface or in an iridium hydride complex to bond to more that one hydrogen atom [14,34]. The TPD profiles (Fig. 6) show that when iridium is present as clusters or aggregates with an average size of about 12 Å or less, only one type of adsorbed hydrogen species is indicated (having a maximum desorption rate at 136°C) (Fig. 6). But when larger iridium aggregates were present, another form of adsorbed hydrogen was evident (having a maximum desorption rate at about 188°C) (Fig. 6). The latter form is more strongly adsorbed than the former. Thus, the TPD data are broadly consistent with the hydrogen chemisorption data, but they do not resolve the issue of why there is a cluster/aggregate size effect on adsorption.

5.6. Catalytic properties of supported tetrairidium clusters for toluene hydrogenation

MgO- [35], γ-Al_2O_3- [4,5], and NaY zeolite- [16] supported iridium clusters, modeled as Ir_4 or Ir_6,

catalyze hydrogenation of cyclohexene and of toluene at 25–60°C. The clusters in the MgO-supported samples had frames indistinguishable from the tetrahedral Ir_4 and remained intact before and after catalysis of toluene hydrogenation, as evidenced by EXAFS spectra of the used catalyst [16]. Spectra of supported Ir_4 and of Ir_6 during propene hydrogenation at 25°C indicate that these clusters were stable during catalysis of this reaction [36].

Furthermore, rates of toluene hydrogenation catalyzed by a family of partially decarbonylated tetrairidium clusters on γ-Al_2O_3 (made by decarbonylation of $[Ir_4(CO)_{12}]$) increased with increasing removal of CO ligands, indicating that only metal sites accessible to reactants facilitate the reaction (Fig. 7) [5]. A qualitatively different pattern was observed for the MgO-supported iridium clusters (Fig. 7). The catalytic reaction rate data characterizing the clusters made by decarbonylation of $[HIr_4(CO)_{11}]^-$/MgO indicate that the catalytic reaction rate increased only gradually with the degree of decarbonylation, except when more than 95% of the CO ligands had been removed, and then the activity increased sharply. The data show that the presence of iridium atoms free of CO ligands is not sufficient for the catalytic reaction to proceed on the MgO-supported clusters. Moreover, the data show that the dependence of the reaction rate on the degree of decarbonylation (Fig. 7) is similar to the dependence of the H/Ir ratio on the degree of decarbonylation (Fig. 8), consistent with the suggestion that the reaction rate depends directly on the amount of hydrogen available on the iridium.

Although the toluene hydrogenation reaction is regarded as structure-insensitive (taking place with roughly the same turnover frequencies on the surfaces of metal particles of different sizes), the turnover frequency for toluene hydrogenation was found to increase as the iridium cluster or particle size on γ-Al_2O_3 increased from about 6 (Ir_4) to about 30 Å, on average [37]. As the larger clusters and particles in this family of samples were formed by H_2-induced sintering of the iridium, one could question whether the data indicate a true cluster size effect or, instead, an effect of removal of surface contaminants (e.g., carbon) as a result of the treatment. The catalytic data representing the Ir/MgO samples having various iridium cluster or aggregate sizes (Table 2) similarly show a significant cluster or aggregate size effect on the toluene hydrogenation rate. The turnover frequency increased by almost two orders of magnitude as the cluster nuclearity increased from four to more than about 100, on average.

5.7. Effect of the support on catalytic activity for toluene hydrogenation

The data reported here and elsewhere [4] are consistent with the expectation that a number of properties (including those of the support) may influence the catalytic activity of a supported metal. The degree of support dehydroxylation apparently affects the catalytic activity of γ-Al_2O_3-supported iridium clusters for toluene hydrogenation [4]. In contrast, when the support was MgO, almost no effect of the surface hydroxyl group density was observed for this reaction [35].

To separate the various support effects from other effects, the catalyst samples to be compared should have the same metal cluster size and structure. Table 6 provides a comparison of the catalytic activities of

Table 6
Toluene hydrogenation catalyzed by iridium clusters on various supports

Support	Support treatment	Decarbonylation conditions	N^a_{Ir-Ir}	Activity, $10^3 \times$ TOF (s^{-1})	Reference
γ-Al_2O_3	Calcination in air at 400°C followed by evacuation at 400°C	He, 300°C	3.0	10.9	[4]
MgO	Calcination in air at 400°C followed by evacuation at 400°C	He, 300°C	3.0	0.3	This work
MgO	Calcination in air at 300°C followed by evacuation at 300°C	He, 300°C	3.7	0.8	[35]

[a] Ir–Ir first-shell coordination number.

iridium clusters with similar nuclearities supported on MgO and on γ-Al_2O_3 that had been dehydroxylated under similar conditions. The data show that the catalytic activity of the γ-Al_2O_3-supported clusters is more than an order of magnitude higher than that of clusters supported on MgO. There are still too few data to show why the γ-Al_2O_3-supported clusters are more active than MgO-supported clusters, but it may be appropriate to invoke the explanation of Lin and Vannice [38–40] for why the activity of Pt/SiO_2–Al_2O_3 is higher than that of Pt/SiO_2 for arene hydrogenation. These authors pointed to the ability of the more acidic mixed oxide support to adsorb the hydrocarbon reactant in close proximity to the platinum particles, where adsorbed species could react with hydrogen activated by platinum. Thus, they suggested that the SiO_2–Al_2O_3 support was not inert but instead played a direct catalytic role. Their suggestion may well account in part for the support effect observed for the iridium cluster catalysts.

6. Conclusions

Interaction of $[Ir_4(CO)_{12}]$ with the surface of partially dehydroxylated MgO leads to the formation of $[HIr_4(CO)_{11}]^-$, as shown by infrared and EXAFS data. MgO-supported $[HIr_4(CO)_{11}]^-$ that had been decarbonylated to various degrees in He or H_2 was characterized by infrared and EXAFS spectroscopies. The EXAFS data indicate that the clusters treated in He essentially retained the Ir_4 frame throughout the decarbonylation process, which was complete at about 300°C, yielding clusters modeled as Ir_4 tetrahedra, with an Ir–Ir first-shell coordination number of 3.0 ± 0.1 and an Ir–Ir distance of 2.67 ± 0.01 Å. When H_2 was used instead of He for the decarbonylation, the iridium clusters aggregated. Infrared data provide evidence that CO ligands react with H_2, resulting in the breaking of C–O bonds.

Partially decarbonylated MgO-supported $[HIr_4(CO)_{11}]^-$ chemisorbed hydrogen. TPD data show that the strength of bonding of hydrogen to the iridium atoms increases with increasing cluster decarbonylation. Completely decarbonylated MgO-supported clusters (modeled as Ir_4) were characterized by relatively low H/Ir and CO/Ir values (e.g. 0.27 and 0.39, respectively). The chemisorption and EXAFS data show that the amount of hydrogen or CO chemisorbed on iridium increases with increasing iridium cluster or aggregate size.

Catalytic hydrogenation of toluene at 60°C and 1 atm was used to determine the dependence of the reaction rate on the degree of cluster decarbonylation. The rate depends on the amount of hydrogen available on the iridium surface and not simply on the degree of decarbonylation. Both the iridium cluster or aggregate size and the nature of the support significantly affect the rate of toluene hydrogenation.

Acknowledgements

This research was supported by the National Science Foundation (grant CTS-9615257). The EXAFS experiments were done at SSRL, which is operated by the Department of Energy, Office of Basic Energy Sciences. The EXAFS data were analyzed with the XDAP software developed by Vaarkamp et al. [6].

References

[1] Oil Gas J. 30 (1992) 30.
[2] D. Rotman, Chem. Week 8 (1992) 150.
[3] B.C. Gates, in: R.D. Adams, F.A. Cotton (Eds.), Catalysis by Di- and Polynuclear Metal Cluster Complexes, Wiley, Weinheim, 1998, p. 509.
[4] O. Alexeev, B.C. Gates, J. Catal. 176 (1998) 310.
[5] O. Alexeev, G. Panjabi, B.C. Gates, J. Catal. 173 (1998) 196.
[6] M. Vaarkamp, J.C. Linders, D.C. Koningsberger, Physica B 208-209 (1995) 159.
[7] E.A. Stern, Phys. Rev. B 48 (1993) 9825.
[8] E.O. Brigham, The Fast Fourier Transform, Prentice-Hall, Englewood Cliffs, NJ, 1974.
[9] F.-S. Xiao, Z. Xu, O. Alexeev, B.C. Gates, J. Phys. Chem. 99 (1995) 1548.
[10] S. Kawi, J.-R. Chang, B.C. Gates, J. Catal. 142 (1993) 585.
[11] S. Kawi, B.C. Gates, Inorg. Chem. 31 (1992) 2939.
[12] S.D. Maloney, F.B.M. Van Zon, M.J. Kelley, D.C. Koningsberger, B.C. Gates, Catal. Lett. 5 (1990) 161.
[13] A.A. Davydov, Infrared Spectroscopy of Adsorbed Species on the Surface of Transition Metal Oxides, Wiley, Chichester, 1990.
[14] G.B. McVicker, J.J. Ziemiak, J. Catal. 95 (1985) 473.
[15] O. Alexeev, D.-W. Kim, G.W. Graham, M. Shelef, B.C. Gates, J. Catal. 185 (1999) 170.
[16] Z. Xu, F.-S. Xiao, S.K. Purnell, O. Alexeev, S. Kawi, S.E. Deutsch, B.C. Gates, Nature (London) 372 (1994) 346.

[17] M. Angoletta, L. Malatesta, G. Caglio, J. Organomet. Chem. 94 (1975) 99.
[18] N.D. Triantafillou, B.C. Gates, J. Phys. Chem. 98 (1994) 8431.
[19] A. Zhao, B.C. Gates, Langmuir 13 (1997) 4024.
[20] N.D. Triantafillou, B.C. Gates, Langmuir 15 (1999) 2595.
[21] R. Bau, M.Y. Chiang, C.Y. Wei, L. Garlaschelli, S. Martinengo, T.F. Koetzle, Inorg. Chem. 23 (1984) 4758.
[22] F.B.M. Van Zon, S.D. Maloney, B.C. Gates, D.C. Koningsberger, J. Am. Chem. Soc. 115 (1993) 10317.
[23] S.E. Deutsch, G. Mestl, H. Knözinger, B.C. Gates, J. Phys. Chem. B 101 (1997) 1374.
[24] A. Zhao, B.C. Gates, J. Catal. 168 (1997) 60.
[25] A. Zhao, B.C. Gates, J. Am. Chem. Soc. 118 (1996) 2458.
[26] W. Guo, J. Liang, J. Hu, Cuihua Xuebao 7 (1986) 219.
[27] W. Guo, C. Xu, Y. Zhou, Y. Chu, J. Liang, Guangpuxue Yu Guangpu Fenxi 5 (1985) 31.
[28] A.K. Smith, A. Theolier, J.-M. Basset, R. Ugo, D. Commereuc, Y. Chauvin, J. Am. Chem. Soc. 100 (1978) 2590.
[29] K. Christmann, G. Ertl, Surf. Sci. 60 (1976) 365.
[30] K. Christmann, G. Ertl, T. Pignet, Surf. Sci. 54 (1976) 365.
[31] H. Ehwald, U. Leibnitz, Catal. Lett. 38 (1996) 149.
[32] F. Lai, D.-W. Kim, O.S. Alexeev, G.W. Graham, M. Shelef, B.C. Gates, Phys. Chem. Chem. Phys. 2 (2000) 1997.
[33] A. Hu, K.M. Neyman, M. Staufer, T. Belling, B.C. Gates, N. Rösch, J. Am. Chem. Soc. 121 (1999) 4522.
[34] B.J. Kip, F.B.M. Duivenvoorden, D.C. Koningsberger, R. Prins, J. Catal. 105 (1987) 26.
[35] S.E. Deutsch, F.S. Xiao, B.C. Gates, J. Catal. 170 (1997) 161.
[36] G. Panjabi, A.M. Argo, B.C. Gates, Chem. Eur. J. 5 (1999) 2417.
[37] F.-S. Xiao, W.A. Weber, O. Alexeev, B.C. Gates, Stud. Surf. Sci. Catal. 101 (1996) 1135.
[38] S.D. Lin, M.A. Vannice, J. Catal. 143 (1993) 539.
[39] S.D. Lin, M.A. Vannice, J. Catal. 143 (1993) 554.
[40] S.D. Lin, M.A. Vannice, J. Catal. 143 (1993) 563.